I&EC research
Industrial & Engineering Chemistry Research

Article

pubs.acs.org/IECR

Systems Design and Economic Analysis of Direct Air Capture of CO_2 through Temperature Vacuum Swing Adsorption Using MIL-101(Cr)-PEI-800 and mmen-Mg_2(dobpdc) MOF Adsorbents

Anshuman Sinha, Lalit A. Darunte, Christopher W. Jones, Matthew J. Realff, and Yoshiaki Kawajiri*

School of Chemical & Biomolecular Engineering, Georgia Institute of Technology, 311 Ferst Drive, Atlanta, Georgia 30332, United States

Supporting Information

ABSTRACT: Direct air capture (DAC) removes CO_2 from the atmosphere and can therefore address sizable nonpoint sources emissions of CO_2 such as those from transportation. We propose a five-step temperature vacuum swing adsorption process for direct air capture using solid adsorbents coated as films on monolithic contactors using steam as the stripping agent during desorption. We perform a modeling study and economic assessment for DAC using two metal organic frameworks, MIL-101(Cr)-PEI-800 and mmen-Mg_2(dobpdc), for which we have experimentally demonstrated film growth on monolith structures. The results indicate minimum energy requirements, and cost estimates are 0.145 MJ/mol-CO_2 and \$75−140/t-CO_2 for MIL-101(Cr)-PEI-800, and 0.113 MJ/mol-CO_2 and \$60−190/t-CO_2 for mmen-Mg_2(dobpdc), respectively. The overall DAC cost is sensitive to adsorbent purchase cost and lifetime as well as cycle parameters such as adsorption and desorption times. We conclude that mmen-Mg_2(dobpdc) has better performance compared to MIL-101(Cr)-PEI-800 in terms of energy requirements because of its higher capacity and nonlinear isotherm.

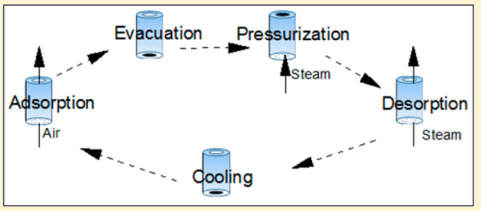

1. INTRODUCTION

The current CO_2 level in the atmosphere is over 400 ppm, as reported by Mauna Loa Observatory, and it continues to rise at a rate of around 2 ppm/yr, driven by anthropogenic emissions mainly from fossil fuel combustion.[1,2] Fossil fuels remain abundant and will continue to be the primary source of energy production for much of the world in the near future. Hence, developing carbon capture utilization and sequestration (CCUS) technologies that act on the atmosphere itself will provide direct control over CO_2 concentrations with the possibility of lowering them over time. CCUS strategies have focused on capturing CO_2 from point sources such as coal-fired power plants or natural gas production wells. These systems focus on removing CO_2 from flue gases and then transporting it to a sequestration site through pipelines, with possible use to enhance oil recovery. However, point sources account for approximately only one-third of the global emissions.[3] In contrast, the strategy explored in this paper is to capture CO_2 directly from ambient air. The advantage of this strategy is that it can capture CO_2 from all emission sources, as direct air capture (DAC) plants can be located anywhere, and specifically can be located either near the site of CO_2 sequestration or the site of CO_2 use. Further, ambient air is cleaner than the flue gas from point sources, where higher concentrations of contaminants such as small particulates and other acid gases such as NO_x and SO can poison the separating agent.

CO_2 capture from air has been researched for more than half a century.[4−6] Lackner et al.[7,8] suggested large scale capture of CO_2 from air as an alternative to CCUS from stationary sources. One proposed approach that has reached pilot scale deployment is to absorb CO_2 using sodium hydroxide solutions.[9−13] There have been several studies[3,14−17] that review DAC technology. Reports by Simon et al.[18] and Smith et al.[19] stressed the need for substantial research into the kinetics of air capture chemistry to reduce cost and energy requirements. House et al.[20] claimed that air capture technology is likely to require more than 400 kJ of work per mole of CO_2 and costs will be on the order of \$1000/t-CO_2. Realff and Eisenberger[21] pointed out a flaw in the analysis of House et al.,[20] stating that because the adsorption capture process is exothermic, the usual scaling of costs with feed dilution do not apply, and the minimum work of capture of CO_2 scales only logarithmically with concentration and is therefore not as serious a barrier as might be expected. A report by the American Physical Society (APS)[22] estimates the cost for both postcombustion capture (PCC) and DAC. The DAC case study was based on a scheme published by Baciocchi, Storti, and Mazzotti[11] which studied CO_2 absorption using a sodium hydroxide solution, and regeneration was performed with the help of a calcium hydroxide solution. It estimated the net cost of DAC to be close to \$610/ton CO_2 captured.

Based on Socolow[22] and the studies mentioned above, one may claim that DAC is economically challenging. However, it is important to note that they considered a particular process (using NaOH) to arrive at their conclusion or used scaling from

Received: October 10, 2016
Revised: December 14, 2016
Accepted: December 19, 2016
Published: December 19, 2016

DOI: 10.1021/acs.iecr.6b03887
Ind. Eng. Chem. Res. 2017, 56, 750−764

other mineral separation technologies. Zeman[23] pointed out that the APS estimates can be significantly reduced from $610 to $309/tCO$_2$ with reduced carbon electricity and plastic packing materials. Other alternatives for capturing CO$_2$ (such as using solid adsorbents like zeolites or MOFs) can be explored since solid sorbents have lower heats of adsorption (45−70 kJ/mol) compared to the heat of reaction of sodium hydroxide and calcination reaction (+200 kJ/mol). These processes have other energy and cost components as well and the conclusion for energy and economic analysis may vary for such processes. Kulkarni et al.[24] analyzed temperature swing adsorption processes for DAC using the purity of CO$_2$ and annual product throughput as a metric for comparing process performance. They used steam as stripping agent to capture CO$_2$ from air using a specific adsorbent TRI-PE-MCM-41. They considered two approaches: One approach was to use diurnal heating and cooling as a driving force for TSA. In the second approach they used steam to provide heat during desorption. They estimated the highest working capacity of the adsorbent as 1.93 mmol/g and the net operating CO$_2$ capture cost up to $100/t-CO$_2$ captured depending on the source of electricity. However, their estimates do not include any information about the capital cost of DAC.

There have been further studies[25−29] that emphasized the potential merits of CO$_2$ capture via the adsorption route. Yu et al.[30] provided a qualitative review on absorption and adsorption processes for CO$_2$ capture. They highlighted the drawbacks of absorption such as high equipment corrosion rate, high energy consumption in regeneration, and need for large absorber volume. Furthermore, they also suggested solid adsorption processes to overcome inherent problems in chemical absorption and highlighted MOFs as promising adsorbents for CO$_2$ capture.

Metal organic frameworks (MOFs) offer large pore volume, tunable pore size, and high specific surface area. They have recently attracted significant attention for use in gas separations.[31−34] Yaghi and Millward[35] first reported MOFs with exceptionally high capacity for CO$_2$ capture at room temperature (298 K). Kuppler et al.[36,37] reviewed the application and progress of MOFs for CO$_2$ capture. MOFs have shown better performance in terms of CO$_2$ uptake and adsorption rate as compared to zeolites.[38,39] MIL-101-(Cr)[25,40−42] and Mg$_2$(dobpdc)[43] (dobpdc^{4-} = 4,4′-dioxido-3,3′-biphenyldicarboxylate) are two MOFs that exhibit excellent CO$_2$ adsorption characteristics at ambient CO$_2$ conditions due to their high density of open metal sites and high pore volume. The cyclic stability of amine loaded MIL-101(Cr) for DAC has been demonstrated in the literature.[25] A series of studies[43−45] reported experimental research on Mg$_2$(dobpdc) to evaluate its performance in CO$_2$ capture. They concluded that the large capacity, high selectivity, and fast kinetics of this material for CO$_2$ adsorption make it an attractive adsorbent for removal of CO$_2$ from air.

Solid sorbents have been used to capture CO$_2$ through temperature, pressure and vacuum swing cycles. In a study by Rezaei et al.,[46] building on earlier work by Lively et al.,[47] a rapid temperature swing adsorption process was developed to predict the performance of postcombustion CO$_2$ capture from flue gas using polymer-supported amine hollow fiber sorbents. In their work, the sensitivity of the model to gas and water velocity and initial temperature was evaluated. They predicted that it is possible to achieve high purity and recovery with a cycle time shorter than 3 min. Casas et al.[48] used PSA technology for precombustion CO$_2$ capture within an integrated gasification combined cycle (IGCC) power plant to perform parametric analysis with activated carbon as the adsorbent material. They carried out multiobjective optimization having CO$_2$ purity and recovery as trade off variables. Wurzbacher et al.[49] demonstrated laboratory-scale capture of CO$_2$ from dry and humid air using a temperature vacuum swing adsorption (TVSA) with the help of packed bed of diamine-functionalized silica gel beads. They studied the effect of parameters such as adsorption time, desorption temperature, etc. on cyclic adsorption capacity. They also predicted specific energy requirements of the TVSA process to be 0.12 MJ/mol CO$_2$ of mechanical work and between 0.49 and 0.64 MJ/mol CO$_2$ of heat, depending on the air relative humidity. Socolow[22] reported a total primary energy requirement of 0.44 MJ/mol for 100% conversion efficiency. In a more recent work by Hefti et al.,[50] a TSA-based model was used to compare the performance of five different metal organic frameworks[45] for postcombustion CO$_2$ capture. They found that the specific energy requirement of the processes with these materials was lower than for a commercial 13X zeolite and similar levels of CO$_2$ purity and recovery could be attained by a lower temperature swing with these materials.

Many alternatives to packed bed systems have been proposed to reduce pressure drop and achieve higher mass throughput. Parallel channel monoliths offer lower pressure drop and higher mass transfer rates than most other mass-solid contactors. The technical feasibility of using parallel channel monoliths for adsorption cycles has already been reported in the literature.[51−53] In studies performed by Rezaei and Webley,[54,55] optimum structures for gas separation processes were explored. Four structured adsorbents, namely, pellet/bead, monolith, laminate, and foam, were analyzed. External surface area, the size of the mass transfer zone, pressure drop and mass transfer rates were considered as trade-off variables. Laminate and monolith structures were finalized as the optimum structures with appropriate spacing and widths for laminate systems and cell densities and voidages for monoliths, respectively. Rezaei et al.[56] studied the impact of monolith wall porosity, channel width distribution and adsorbent film thickness on the dynamic behavior of zeolite coated 400 and 1200 cell per square inch (cpsi) monolith adsorbents for CO$_2$ adsorption. They demonstrated the advantage of zeolite coated monoliths with low wall porosity for gas separation processes. Thus, literature studies[51−55] suggest that monoliths can be considered a feasible option as a support structure for coating MOF films.

There have been a few studies on the application of steam as the stripping agent for CO$_2$ capture.[57−60] Li et al.[61] carried out lab scale experiments to analyze the stability of three classes of supported amine sorbents under steam stripping conditions during the desorption step. These sorbents were subjected to cyclic adsorption and desorption tests using CO$_2$ diluted in N$_2$ and then regenerating the sorbents by contacting them with pure saturated steam with the flow rate at 1.2 g/min at 103 °C for 25 min. They have demonstrated that amine adsorbents can show stability in cyclic adsorption/desorption experiments using steam stripping.

The studies discussed above provide useful insights into the development of CO$_2$ capture technologies. However, no study has yet reported detailed cost and energy analysis of DAC through modeling of a process that employed temperature vacuum swing adsorption on monolith structures coated with MOF films. In this paper, we propose to evaluate the performance of MIL-101(Cr)-PEI-800[25] and mmen-

DOI: 10.1021/acs.iecr.6b03887
Ind. Eng. Chem. Res. 2017, 56, 750−764

$Mg_2(dobpdc)$[45] MOF materials by performing detailed economic and energy analysis of a DAC process employing these two adsorbents. Two case studies (one for each adsorbent) have been performed and temperature vacuum swing adsorption has been used in each of these case studies to remove CO_2 from the adsorbent film coated on monolithic contactors with the help of saturated steam as the stripping agent. The outcome of this modeling effort is used to optimize the TVSA operation conditions and to provide guidance on materials development to improve the performance of the DAC process. In this paper, a set of numerical models for a cyclic TVSA process is developed and the effect of the air and steam velocity on the concentration and temperature profiles of the DAC system are analyzed accordingly.

2. PROCESS DESCRIPTION

We consider a cyclic TVSA process comparing MIL-101(Cr)-PEI-800[25] and mmen-$Mg_2(dobpdc)$[43,45] as adsorbents coated inside cordierite monolith channels. Figure 1 shows an overall

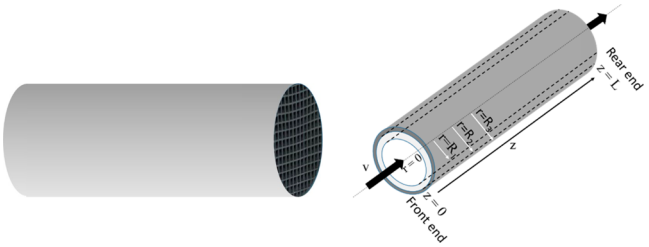

Figure 1. Monolithic support structure with multiple channels (left) and schematic of a single monolithic channel (right).

view of a monolith support structure with an enlarged schematic of a single monolithic channel, which we assume to be cylindrical for convenience in this analysis. Each monolithic channel is coated with an adsorbent film. The thickness of the adsorbent film is around 60 μm (section 6.1) and each monolith channel is around 1270 μm in diameter ($2R_3$) which corresponds to a cell density of 400 cpsi (section 6.1).

We propose a five step TVSA cycle as illustrated in Figure 2. In the adsorption step (Step 1), air is passed through the channel at ambient conditions (298 K, 1 atm, and 25% relative humidity). The CO_2 concentration in the air is 400 ppm. This corresponds to a molar concentration of 0.016 mol/m^3. The adsorbent film starts adsorbing this CO_2 during this step, and in cyclic steady state, condensed water is evaporated from the channel surface at the start of the step.

The second step is to evacuate the channel, since it is filled with air (containing oxygen) at the end of adsorption step. This step is required since the amine groups in the MOFs may be oxidized[62,63] at higher temperatures. Hence, the oxygen concentration in the channel must be lowered during the evacuation step. This is achieved by closing the front end (z = 0) of the channel and evacuating it by decreasing the pressure at the rear end ($z = L$) with the help of a vacuum pump. This step is finished once the oxygen concentration inside the channel falls below 4% since at that oxygen concentration and at 373 K, the amine groups in MOFs have been observed not to be oxidized to any significant extent.[63] It is assumed that the vacuum is pulled rapidly and that the dynamics of the mass transfer from the MOF does not allow CO_2 to desorb from the surface.

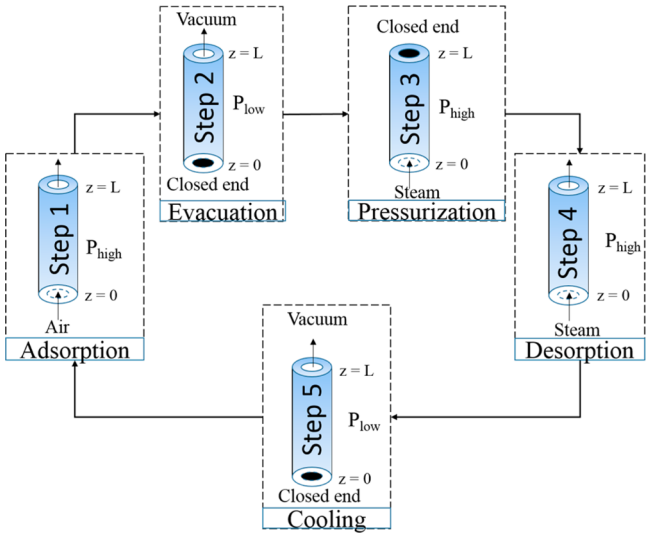

Figure 2. Overview of the steps involved in the TVSA model for DAC.

The third step is to pressurize the channel to 1 atm to prevent any backflow of air (oxygen) from the rear end ($z = L$) of the channel. This is done by closing the rear end of the channel and passing saturated steam at 1 atm through the front end (z = 0) until the entire channel is pressurized; this happens very rapidly.

For the desorption step (step 4), the rear end ($z = L$) of the channel is opened and saturated steam at 1 atm is fed to the channel from the front end (z = 0). The steam condenses on the surface of the adsorbent, increasing its temperature. This results in CO_2 desorption during this step due to the temperature swing.

The last step (cooling) of the TVSA cycle is to cool the system down to 348 K. This step is essential because at the end of desorption step, the system is at 373 K. This poses the risk of oxidative degeneration of amine groups in the adsorbent if we start flowing the air (step 1) through the channel. Hence, it is necessary to bring the channel temperature down, and we have used 348 K since the amine groups do not show significant oxidative degeneration when the temperature is in this range.[63] To achieve this, we close the front end (z = 0) of the channel and decrease the pressure at the rear end ($z = L$) so that the water condensed on the adsorbent surface evaporates, thereby cooling the adsorbent.

3. MODEL EQUATIONS

A mathematical model has been developed to simulate the DAC process to capture temperature and concentration dynamics of the TVSA model. The following assumptions were made to develop the mathematical model:

- Air is considered to have oxygen and nitrogen components in addition to the CO_2 (and 25% relative humidity) and the saturated steam is pure.
- Ideal gas law and ideal mixtures are assumed for the noncondensible components.
- Temperature and concentration variations are neglected in the radial direction in the adsorbent film and monolith wall leading to a lumped model in the radial coordinate for these model elements.
- Adsorbent film thickness is uniform in the axial direction.
- During the desorption step, condensed water does not penetrate inside the MOF pores due to high flow rate of

DOI: 10.1021/acs.iecr.6b03887
Ind. Eng. Chem. Res. 2017, 56, 750−764

desorbed CO_2 from the MOF pores in the opposing direction. Thus, heat is conducted into the MOF and wall and is not transferred by diffusion of steam within the MOF phase following steam condensation.
- Heat loss from the channel is negligible during all steps of the cycle.

On the basis of the above assumptions, a differential mass and heat balance equation can be written for the TVSA model[64] (refer to section S1 in the Supporting Information).

The pressure drop across the channel is given by the Hagen−Poiseuille equation:[64]

$$\Delta P = \frac{8L\mu v}{R_1^2} \quad (1)$$

where L is the length of the channel, v is the velocity of gas inside the channel, μ is the gaseous viscosity, and R_1 is channel inner radius. The other source of pressure drop is due to drag on the system, which is estimated by

$$P_d = \frac{1}{2}\rho v^2 c_d \quad (2)$$

where, P_d is the pressure drop due to bluff body drag, ρ is the density of the gas, and c_d is the drag coefficient. This pressure drop should overestimate the drag as the monolith is porous. For this system, the pressure drop due to drag (eq 2) is estimated to be negligible as compared to the standard pressure drop given by the Hagen−Poiseuille equation (eq 1).

The CO_2 adsorption rate is approximated by the linear driving force model[65] as given by

$$\frac{\partial Q_{CO_2}}{\partial t} = k(Q^{eq}_{CO_2} - Q_{CO_2}) \quad (3)$$

where, Q_{CO_2} is the adsorbed CO_2 concentration. $Q^{eq}_{CO_2}$ and k are the equilibrium concentration of CO_2 as determined by isotherm equations and overall mass transfer coefficient,[65] respectively, which are determined quantitatively in section 6.1.

The condensation step is modeled assuming the difference between the bulk concentration of water vapor molecules and its concentration at the interface is the driving force for water condensation (eq 4). The mass transfer constant was calculated using the correlation given by Jeong et al.[66] The concentration at the interface is assumed to be in equilibrium with pure liquid water and thus estimated using the Antoine equation (eq 5).

$$-D_{H_2O}\frac{\partial C_{H_2O}}{\partial r}_{|r=R_1} = k_m(C_{H_2O} - C^i_{H_2O}) \quad (4)$$

$$C^i_{H_2O} = \frac{\exp\left[a - \left(\frac{b}{T_{gas}+c}\right)\right]}{RT_{gas}} \quad (5)$$

where $C^i_{H_2O}$ is the saturation concentration of water vapor at the MOF-channel interface, and a, b, and c are the Antoine constants given in Table 1.

The heats of adsorption for CO_2 were determined using the Clausius−Clapeyron equation at 25, 50, and 75 °C. They were calculated to be around 55 kJ/mol for MIL-101(Cr)-PEI-800 and 70 kJ/mol for mmen-Mg_2(dobpdc) (refer to S4 in the Supporting Information).

The system design specifications and mass and heat transfer properties are tabulated in Table 1 and Table 2, respectively.

Table 1. System Properties for TVSA CO_2 Capture

name	symbol	value
air thermal conductivity (W/m K)	k_g	0.0257
air heat capacity (J/(kg K))	$C_{p,g}$	1003
air density (kg/m^3)	ρ_g	1.1839
adsorbent thermal conductivity (W/(m K))	k_{ads}	0.32[67,68]
adsorbent heat capacity (J/(kg K))	$C_{p,ads}$	892.5[67,69]
adsorbent density (kg/m^3)	ρ_{ads}	500[67]
wall thermal conductivity (W/(m K))	k_{wall}	1.6[70]
wall heat capacity (J/(kg K))	$C_{p,wall}$	840[71]
wall density (kg/m^3)	ρ_{wall}	2050[70]
Antoine constants	a, b, c	5.2, 1733.9, −39.5[72]

Table 2. Mass and Heat Transfer Properties

parameter	value
D_g (m^2/s)	0.000016
h (W/m^2-K)	75
$T_{ambient}$ (K)	298
$C_{CO_2,0}$ (mol/m^3)	0.016
C_{inert_0} (mol/m^3)	40.88
ΔH (J/mol)	55000 (MIL-101(Cr)-PEI-800)
ΔH (J/mol)	70000 (mmen-Mg_2(dobpdc))
A_1 (m)	0.000063
A_2 (m)	0.000052

4. ESTIMATION OF ENERGY REQUIREMENTS

To estimate the feasibility of the DAC process through the proposed TVSA model, it is essential to analyze the energy requirements of the process. The air is assumed to be moved via an electrically driven fan during the adsorption step (step 1). Higher air flow rates cause a larger pressure drop across the channel and hence a higher load on the fan. The energy requirement of the fan (E_1) is the product of pressure drop required across the channel and the net volumetric air flow during the adsorption step. During the evacuation step (step 2), energy is required by the vacuum pump (E_5) to decrease the pressure inside the channel from 1 to 0.2 atm. During the desorption step (step 4), energy is required to provide sensible heat to the adsorbent (E_2), the monolithic wall (E_3) for desired temperature rise, and to desorb adsorbed CO_2 molecules (E_4). Energy is also embodied in the uncondensed steam (E_6) that exits the monolith channel during the desorption step. During the cooling step (step 5), vacuum pumps are used (E_5) to lower down the partial pressure of water vapor inside the channel.

The sum of these energies ($E_1 + \cdots + E_6$) gives the total energy used by the system. The theoretical minimum energy requirement of the system is defined by the sum of E_1 to E_5, as the steam that is uncondensed is effectively wasted unless this low temperature enthalpy can be recovered. We discuss both the total energy used by the system and the minimum energy required by the system in section 6.3.

Table 3 describes the equations used to estimate the energy requirements. E refers to the energy required in joules per mole of CO_2 removed. Q_{step_1} and t_{step_1} are the gas flow rate and time taken during Step 1 of the TVSA cycle and m_{ads} and m_{wall} are the mass of the adsorbent and monolithic wall per channel, respectively. P_1 is the initial pressure and V_2 and V_1 are the final and initial volume, respectively, during the vacuum swing steps (evacuation and cooling steps). L' is the latent heat of low grade steam (as explained in section 6.3). Derivation of these

DOI: 10.1021/acs.iecr.6b03887
Ind. Eng. Chem. Res. 2017, 56, 750−764

Table 3. Energy Requirements for the TVSA Model

components	energy requirements (in Joules per mole CO_2 captured)
electrical energy for blowers	$E_1 = \Delta P Q_{step\,1} t_{step\,1}/N_m$
adsorbent sensible heat	$E_2 = \frac{m_{ads} C_{p,ads}}{L N_m} \int_{t=t_{step\,4}}^{t_{step\,5}} \left(\int_{z=0}^{L} \frac{dT_{ads}}{dt} dz \right) dt$
monolithic wall sensible heat	$E_3 = \frac{m_{wall} C_{p,wall}}{L N_m} \int_{t=t_{step\,4}}^{t_{step\,5}} \left(\int_{z=0}^{L} \frac{dT_{wall}}{dt} dz \right) dt$
CO_2 desorption heat	$E_4 = \Delta H$
electrical energy for vacuum pump	$E_5 = -\frac{P_1 V_1^{\gamma}}{N_m} \frac{(V_2^{1-\gamma} - V_1^{1-\gamma})}{1-\gamma}$
energy in uncondensed steam	$E_6 = \frac{2\pi L'}{N_m} \int_{t=t_{step\,4}}^{t_{step\,5}} \left(\int_{r=0}^{R_1} v_{step\,4} r C_{H_2O}(L)\, dr \right) dt$

energy requirements is provided in S2 in the Supporting Information. Detailed results and analysis of the energy requirements of the TVSA model are provided later (section 6.3). We assume a pump efficiency of 85% in this analysis.

N_m is the amount of CO_2 captured (in moles) per channel per cycle, as given by eq 6:

$$N_m = m_{ads} \int_{t_{step\,4}}^{t_{step\,5}} \int_{0}^{L} \frac{dQ_{CO_2}}{dt} dz\, dt \tag{6}$$

5. ESTIMATION OF COST

The total cost of DAC can be split into operating and capital costs. To place these on the same basis, we will use the normal procedure of finding an annualized capital cost (annualized over 10 years lifetime for the monolith, blower, and vacuum pump and 1−3 years lifetime for the adsorbents), and use a basis of 1 tonne of CO_2 captured. We assume a 1.1 × 1.1 × 0.3 m contactor, which results in 750 000 channels per contactor (for 400-cpsi monolith). The capital cost consists of mainly adsorbent, monolith, fans, and vacuum pump costs.

Table 4 describes the equations used to estimate each of these costs. $Q_{step\,1}$ and $Q_{step\,4}$ are the gas flow rate during step 1 (adsorption step) and step 4 (desorption step) of the TVSA cycle, respectively. $t_{step\,1}$, $t_{step\,4}$ and t_{cycle} are the time taken (in seconds) during step 1, step 4, and the entire TVSA cycle, respectively, and t_{yr} is the time (in seconds) in 1 year, assuming 330 days of operation per year. C_E ($/kW-hr), C_{st} ($ per unit weight of steam), and C_{ads} ($ per unit weight of adsorbent) are the purchase costs of electricity, steam, and adsorbent, respectively. $C_{monolith}$ ($ per cubic inch of monolith substrate), C_B ($), C_{Vac} ($) and C_M ($) are the bare module costs of the monoliths, blowers, pumps, and electric motor, respectively. $V_{monolith}$ and m_{ads} are the volume of one monolithic channel and mass of the adsorbent per channel, respectively. N_t is the amount of CO_2 removed (in tonnes) per channel per cycle and $N_{yr,i}$ is the lifetime of the individual components. We assume that the steam is provided from a main steam system and there is no capital recovery charge for the steam use. This was done to avoid the complexity of designing and building a standalone combined heat and power (CHP) system or another means for providing the steam to the plant, such as a solar thermal cycle. Derivation of these costs is provided in the Supporting Information. (refer to section S3). Detailed analysis of the cost of the system with MIL-101(Cr)-PEI-800 and mmen-Mg_2(dobpdc) as the adsorbents is provided later. (section 6.4)

Table 4. Cost Calculations for the TVSA Model

components	operating cost (dollars per tonne)
fan	$C_1 = \Delta P Q_{step\,1} t_{step\,1} C_E/N_t$
steam	$C_2 = Q_{step\,4} t_{step\,4} \rho_{st} C_{st}/N_t$
vacuum pump	$C_3 = \frac{E_5 N_m}{N_t}$
components	**capital cost (dollars per tonne)**
monolith	$C_4 = V_{monolith} \frac{C_{monolith} t_{cycle}}{N_t N_{yr_1} t_{yr}}$
adsorbent	$C_5 = m_{ads} \frac{C_{ads} t_{cycle}}{N_t N_{yr_2} t_{yr}}$
blower	$C_6 = \frac{C_B t_{cycle}}{N_t N_{yr_3} t_{yr}}$
vacuum pump	$C_7 = \frac{(C_{vac} + C_M) t_{cycle}}{N_t N_{yr_4} t_{yr}}$

The steam operating cost is estimated from the steam required, and hence lost power production, in a steam turbine system because air capture has been added to the turbine system. In our case, we assume that the turbine system is not increased in size and that steam is diverted from making power in the condensing turbine. Therefore, we included the cost of the lost power because the steam could not be put through this final expansion step. The cost of the electricity for the fans and vacuum pumps is taken to be the same value as that for the lost generating capacity.

6. RESULTS AND DISCUSSION

The cyclic TVSA model has been implemented in gPROMS version 4.0. The model was solved by discretizing the axial and radial domain using the second order centered finite difference method (CFDM). The method of lines was used to solve the partial differential algebraic equations, and the DASOLV integrator was used to solve the resulting equations. The number of spatial finite elements was increased gradually until no further change in the profiles was observed within a percent error of 10^{-7}. This resulted in 1500 and 3500 finite elements in the axial domain for mmen-Mg_2(dobpdc) and MIL-101(Cr)-PEI-800, respectively, and three elements in the radial domain for the gas channel for both the adsorbents. Further, the MATLAB lsqnonlin solver was used for nonlinear curve fitting for parameter estimation of isotherm equations from data points obtained from experiments.

6.1. Isotherm Parameter Fitting. CO_2 adsorption isotherms at different temperatures were measured using MIL-101(Cr)-PEI-800m which had a capacity of 1 g of CO_2/mmol sorbent at 400 ppm of CO_2 concentration. Experimental details can be found in Darunte et al.[25] The experimental data from the isotherm measurement of MIL-101(Cr)-PEI-800 were used to estimate the parameters for CO_2 adsorption using a temperature dependent isotherm model (eq 7). Figure 3 shows a good agreement between the model equation and experimental data, with a R^2 value of 0.99. The estimated model parameters are presented in Table 5. Equation 7 represents the isotherm that is considered to represent the adsorption equilibrium for MIL-101(Cr)-PEI-800.

DOI: 10.1021/acs.iecr.6b03887
Ind. Eng. Chem. Res. 2017, 56, 750−764

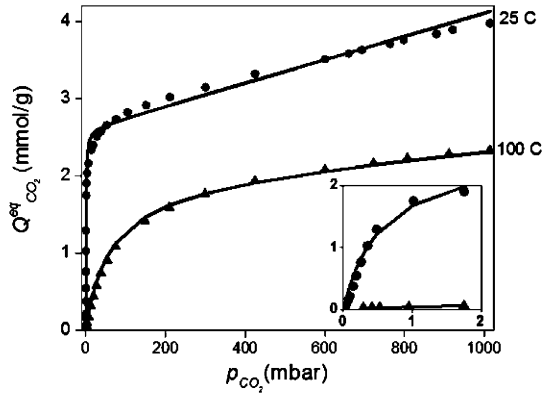

Figure 3. Model fitting of isotherm data for the MIL-101(Cr)-PEI-800 adsorbent.

$$Q^{eq}_{CO_2} = \frac{q_{sat_1} b_1 p_{CO_2}}{1 + (b_1 p_{CO_2})} + b_2 p_{CO_2} \tag{7}$$

Table 5. Isotherm Parameters for the MIL-101(Cr)-PEI-800 Adsorbent

parameter	298 K	323 K	348 K
q_{sat_1} (mmol/g)	2.6	2.4	1.9
b_1 (mbar^{-1})	1.8	0.3	0.02
b_2 (mmol/g-mbar)	0.0015	0.00096	0.00046

In addition, experimental data published previously[45] has been used to estimate the isotherm parameters for mmen-Mg_2(dobpdc). As can be seen from Figure 4 (subplot), the

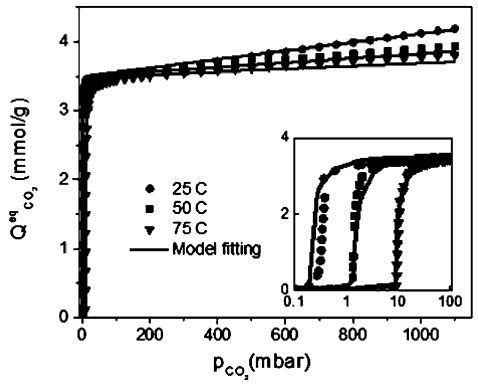

Figure 4. Model fitting of isotherm data for mmen-Mg_2(dobpdc) for (a) the entire pressure range and (b) the low pressure range.

isotherm exhibits an S-shaped behavior at low CO_2 partial pressure. To model such a behavior, hybrid model eqs 8 and 9 are proposed. Equation 8 is used for model fitting for the region before the step pressure and eq 9 fits the model for the region after the step pressure (see section S4 of the Supporting Information):

$$Q^{eq}_{CO_2,1} = \frac{q_{sat,2} b_3 p_{CO_2}}{1 + b_3 p_{CO_2}} \qquad (p_{CO_2} < p_{step}) \tag{8}$$

$$Q^{eq}_{CO_2,2} = \frac{q_{sat,3} b_4 (p_{CO_2} - p_{step})}{1 + b_4 (p_{CO_2} - p_{step})} + b_5 p_{CO_2} \qquad (p_{CO_2} > p_{step}) \tag{9}$$

where $q_{sat,i}$ and b_i are the isotherm parameters (Table 6) and p_{step} is the pressure at which the step in the isotherm occurs

Table 6. Isotherm Parameters for the mmen-Mg_2(dobpdc) Adsorbent

parameter	298 K	323 K	348 K
Before Step Pressure			
q_{sat_2} (mmol/g)	0.16	0.16	0.16
b_3 (mbar^{-1})	4.89	1.20	0.36
After Step Pressure			
q_{sat_3} (mmol/g)	3.50	3.50	3.50
b_4 (mbar^{-1})	22.00	3.56	0.75
b_5 (mmol/g-mbar)	0.00062	0.00033	0.00019
p_{step} (mbar)	0.16	1.33	8.26
p_{step0}	0.62	0.62	0.62
H_{step}	68000	68200	68200
T_0	313.5	313.5	313.5

(step pressure). It can be seen from Figure 4 that there is a good agreement between the model equation and experimental data with a R^2 value of 0.96.

Figure 4 (subplot) shows that the step pressure changes that occur with the change in temperature. The temperature dependence of the step pressure (eq 10) is taken from McDonald et al.,[45] with the parameters reported in Table 6.

$$p_{step} = p_{step0} \exp\left(\frac{-H_{step}}{R}\left[\frac{1}{T_0} - \frac{1}{T_{gas}}\right]\right) \tag{10}$$

6.2. TVSA Model Results. In this section, we compare the results of the base case TVSA model for both adsorbents, using the parameters for the monolith in Table 7 and the operating

Table 7. Systems Design Parameters for the TVSA Cycle CO_2 Capture

name	unit	value
monolith cell density		400 cpsi
channel outer radius	μm	635
monolith wall thickness	μm	50
adsorbent film thickness	μm	60
channel length	m	0.3
overall mass transfer coefficient, k	s^{-1}	0.005
effective diffusivity, D_e	m^2 s^{-1}	10^{-11}[73−75]
Reynolds number, Re		190
Schmidt number, Sc		17

parameters in Table 8. We present the results for the adsorption step (step 1), desorption step (step 4) and cooling step (step 5). The evacuation (step 2) and pressurization (step 3) steps are almost instantaneous (refer to section S6 of the Supporting Information for additional details on step 2 and step 3).

6.2.1. Adsorption Step. The simulated breakthrough profiles and adsorbed phase concentration fronts for both MIL-101(Cr)-PEI-800 and mmen-Mg_2(dobpdc) are presented in Figure 5. The adsorption step is simulated for 6000 s for both

DOI: 10.1021/acs.iecr.6b03887
Ind. Eng. Chem. Res. 2017, 56, 750−764

Table 8. TVSA Operating Conditions

parameter	value (MIL-101(Cr)-PEI-800)	value (mmen-Mg_2(dobpdc))
v_{step1} (m/s)	3.0	3.0
v_{step4} (m/s)	0.04	0.1
t_{step1} (s)	1150	3600
t_{step4} (s)	1230	900
t_{step5} (s)	60	60
t_{cycle} (= t_{step1} + t_{step4} + t_{step5}) (s)	2440	4560

the adsorbents at the cyclic steady state, utilizing effectively the full adsorption equilibrium of both the adsorbents (for comparison purposes).

Comparing the dynamics of the CO_2 breakthrough fronts for both the adsorbents (shown in Figure 5a) under the same operating conditions, MIL-101(Cr)-PEI-800 undergoes an earlier breakthrough as compared to mmen-Mg_2(dobpdc). Similarly, Figure 5b compares the average adsorbed CO_2 in the adsorbent film during the adsorption step for both the adsorbents. The average amount of CO_2 adsorbed in the adsorbent is defined as

$$Q_{avg} = \frac{\int_0^L Q_{CO_2}\, dz}{L} \tag{11}$$

These results follow directly from the difference in the saturation capacities of the two adsorbents. mmen-Mg_2(dobpdc) has a higher saturation capacity (~2.9 mmol/g) than MIL-101(Cr)-PEI-800 (~1 mmol/g) at ambient conditions, (1 mmol/g adsorbent capacity corresponds to 64.8 mmol/m^3 of monolithic contactor) Also, in the same figure, the mmen-Mg_2(dobpdc) breakthrough front exhibits shock wave behavior.[76] This is due to the hybrid isotherm shape and model (eqs 8 and 9 for mmen-Mg_2(dobpdc).

6.2.2. Desorption Step. During the desorption step, the saturated steam causes an increase in temperature of the channel. The steam condenses at 373 K upon contacting the adsorbent film, resulting in heat transfer from the condensed water to the adsorbent surface. Figure 6a shows the variation of the adsorbent temperature at the channel exit for both the adsorbents. Keeping the steam velocity at 0.04 m/s (for MIL-101(Cr)-PEI-800) and 0.1 m/s (for mmen-Mg_2(dobpdc)), the desorption step is simulated for 1500 s for both the adsorbents at the cyclic steady state, utilizing the full desorption potential of both the adsorbents (for comparison purposes). It can be seen from the figure that the temperature increased from 298 to 373 K for both the adsorbents during the desorption step.

It takes some time before the temperature starts increasing during the desorption step, as seen from Figure 6a. This is because this analysis is shown at the channel exit ($z = L$). It takes time before the steam reaches the channel exit, and by keeping the steam velocity at 0.04 m/s (for MIL-101(Cr)-PEI-800) and 0.1 m/s (for mmen-Mg_2(dobpdc)), it is ensured that the steam concentration front is always behind the desorbed CO_2 front. This minimizes the use of steam at the expense of having a longer desorption time, rolling the CO_2 along the channel, increasing its concentration as it proceeds.

Figure 6b shows the variation of the amount of CO_2 (in moles) adsorbed per channel for both the adsorbents. The total amount of CO_2 captured per channel per cycle by mmen-Mg_2(dobpdc) is higher than by MIL-101(Cr)-PEI-800 since mmen-Mg_2(dobpdc) has a higher equilibrium capacity than MIL-101(Cr)-PEI-800 at ambient conditions. This can be further confirmed from Figure 6b, which shows that the initial amount of CO_2 adsorbed for mmen-Mg_2(dobpdc) is almost triple that of MIL-101(Cr)-PEI-800, and mmen-Mg_2(dobpdc) shows a steeper slope at the end of this step.

Figure 7a and b compare the adsorbent temperature, desorbed CO_2 gaseous concentration, and water vapor concentration in the channel at the cyclic steady state at 110 s for MIL-101(Cr)-PEI-800 and 30 s for mmen-Mg_2(dobpdc) during the desorption with a steam velocity of 0.04 m/s (for MIL-101(Cr)-PEI-800) and 0.1 m/s (for mmen-Mg_2(dobpdc)). It is evident from both the figures (Figure 7a,b), that the steam concentration front is behind the desorbed CO_2 concentration front. This indicates that the steam is condensed and the latent heat is used effectively to desorb CO_2 at the concentration front, thereby minimizing the steam consumption.

6.2.3. Cooling Step. The cooling step should be designed such that the adsorbent is cooled to a sufficiently low temperature (~348 K) before the air flow is started for the adsorption step. To overcome this issue, during the cooling step, the front end of the channel is closed and pressure is decreased gradually from the rear end with the help of a vacuum pump. This decreases the partial pressure of water vapor inside the channel, causing the water condensed on the

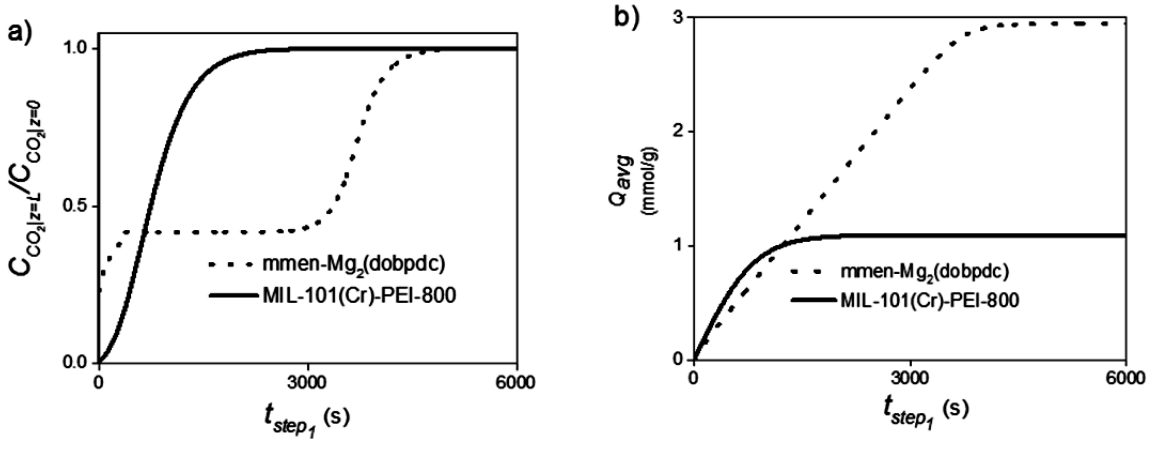

Figure 5. (a) CO_2 breakthrough profile and (b) adsorbed average CO_2 concentration.

DOI: 10.1021/acs.iecr.6b03887
Ind. Eng. Chem. Res. 2017, 56, 750−764

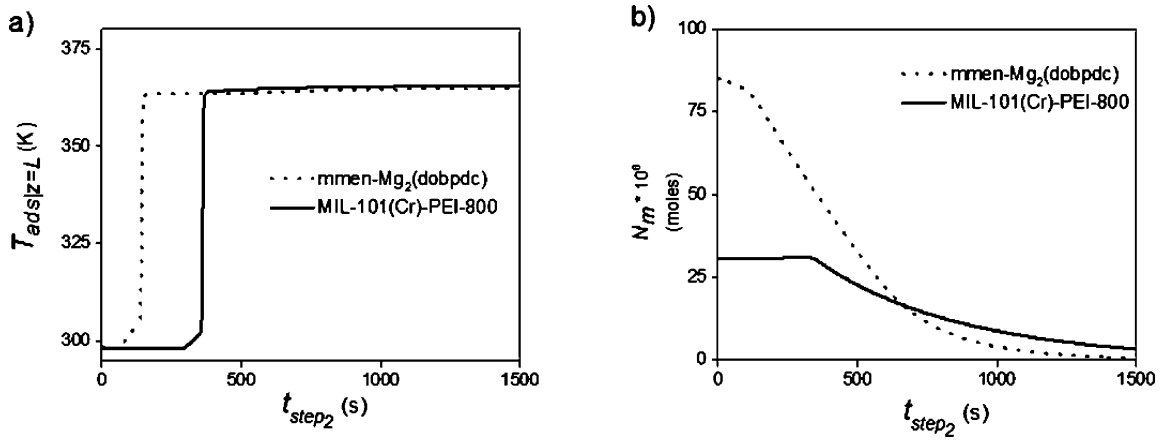

Figure 6. Variation of (a) the adsorbent exit temperature and (b) the total CO_2 moles adsorbed per channel during the desorption step.

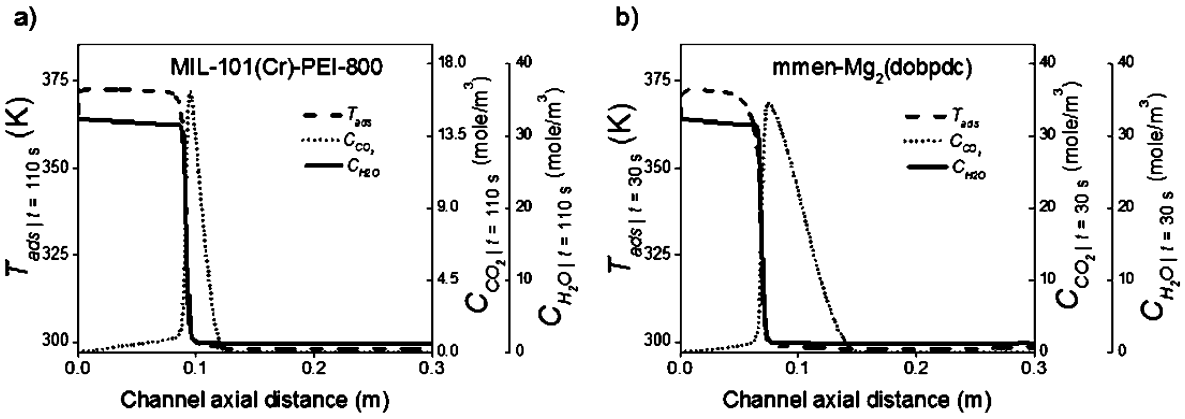

Figure 7. Comparison of adsorbent temperature, CO_2 gaseous concentration and water vapor concentration in the channel at 200 s during the desorption step for (a) MIL-101(Cr)-PEI-800 and (b) mmen-Mg$_2$(dobpdc).

adsorbent surface to evaporate, thereby decreasing the temperature of the system. This continues until the adsorbent temperature has decreased to 348 K. To achieve this temperature, the pressure inside the channel needs to be lowered to 0.4 atm.

The adsorbent temperature dynamics at the channel exit during the cooling step at the cyclic steady state are presented in Figure 8. It can be seen from the figure that it takes 60 s for the channel temperature to cool to 348 K. It is evident from the figure that both the adsorbents exhibit similar decreases in adsorbent temperature. This is because the system size and operating conditions are similar for both adsorbents during the cooling step. Hence, the rate of cooling is similar for both.

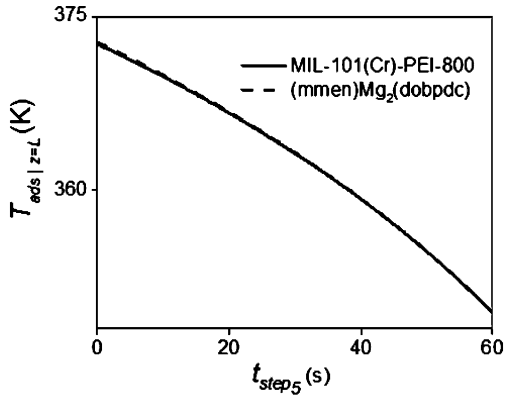

Figure 8. Adsorbent temperature variation for both adsorbents during the cooling step.

6.3. Energy Analysis. In section 4, we discussed the approach to estimate the energy requirement of the TVSA system for DAC. In this section, we use the equations from section 4 to perform a detailed analysis of the energy requirements. For this analysis, we use a "primary combustion energy" basis where all the energy requirements are moved back through a supply chain into a fossil energy source in the ground that would correspond to the final delivered energy for the process. This allows us to put electricity, steam, and fuel use on a common basis and to compare them to the energy available when combusting carbon. For the latter comparison to be made, a representative form of fossil carbon has to be chosen relative to its composition, or state of reduction. Following,[8] we choose CH_2 as the basis for comparison with a heat of combustion of 0.45 (MJ/mol carbon as CH_2). This provides an upper bound on the combustion energy we should expend to capture a mole of CO_2.

For simplicity, we assume the steam would come from a steam turbine system running from 753 K and 65 bar to 408 K and 1.1 bar, which are reasonable conditions at the inlet of a high pressure and condensing steam turbine, respectively. The steam for the desorption would be extracted before the remaining steam is sent to a condensing turbine. Thus, we consider the difference in electricity generation between two systems, one with and one without a condensing turbine, as the

DOI: 10.1021/acs.iecr.6b03887
Ind. Eng. Chem. Res. 2017, 56, 750−764

energy penalty of the air capture system. The decreased electricity can be translated to a fuel use by using an efficiency of electricity generation. A scale up factor[77] of 3.14 and 1.20 have been used to convert electrical and thermal energy respectively to primary combustion energy. Table 9 below gives the assumptions for the steam system, additional efficiency factors, and energy requirements for the system.

Table 9. Assumptions for the Steam System, Efficiency Factors, and Primary Combustion Energy Requirements

steam inlet condition	753 K and 65 bar
steam outlet condition	408 K and 1.1 bar
boiler efficiency (%)	85
turbine isentropic efficiency (%)	70
loss of electricity generation per kg of steam	0.14 MJ/h

primary combustion energy requirements (MJ/mol)	MIL-101(Cr)-PEI-800	mmen-Mg_2(dobpdc)
energy consumed by blowers (E_1)	0.1	0.09
adsorbent sensible heat (E_2)	0.006	0.002
monolithic wall sensible heat (E_3)	0.022	0.006
energy due to CO_2 desorption (E_4)	0.006	0.005
energy consumed by vacuum pumps (E_5)	0.010	0.010
minimum primary combustion energy requirements ($E_1 + \cdots + E_5$)	0.145	0.113
energy due to uncondensed steam (E_6)	0.080	0.045
net primary combustion energy used ($E_1 + \cdots + E_6$)	0.225	0.158

Table 9 presents an analysis of the energy requirements for the MIL-101(Cr)-PEI-800 and mmen-Mg_2(dobpdc) adsorbents. It can be noted that the energy requirement for the MIL-101(Cr)-PEI-800 is higher than that for the mmen-Mg_2(dobpdc) adsorbent. Here, the energy requirements for these two materials are evaluated by comparing them with the minimum theoretical energy use: the energy required for unmixing of two ideal gases, inert and CO_2, is around 0.02 MJ/mol for CO_2 at atmospheric concentrations.[22] A benchmark for the maximum energy use that would lead to a net negative CO_2 balance in the atmosphere is the 0.45 kJ/mol given earlier. It can be seen from Table 9 that the minimum primary combustion energy requirements for the MIL-101(Cr)-PEI-800 and mmen-Mg_2(dobpdc) adsorbents are around 0.145 MJ/mol and 0.113 MJ/mol, respectively. We assume 100% thermal efficiency to calculate these values. However, for a process with a thermal efficiency of 85%, the minimum primary combustion energy requirements for the MIL-101(Cr)-PEI-800 and mmen-Mg_2(dobpdc) adsorbents are around 0.150 MJ/mol and 0.125 MJ/mol, respectively. This means that this process does require less primary combustion energy than the primary combustion energy available in the carbon using these process conditions and assumptions on the form of the carbon fuel. The energy loss from the channel boundary has been assumed to be negligible compared to other energy consumption terms.

6.4. Net Cost Analysis. The procedure to estimate the cost of the TVSA model for DAC process is explained in section 5. In this section, we have performed a preliminary economic analysis based on the equations in section 5.

The cost of the adsorbent and its lifetime are two additional parameters that affect the overall cost of the DAC process. We assume the purchase cost (C_{ads}) of MIL-101(Cr)-PEI-800 and mmen-Mg_2(dobpdc) to be \$15/kg and \$50/kg, respectively (refer S3 in the Supporting Information).[78] This assumes the bulk price of reagents with 100% product yield and includes raw material, labor, maintenance, and utility costs required for the adsorbent production. The cost coefficient may increase or decrease from the value assumed above if the adsorbent synthesis has lower yield or is made more efficiently. To account for this uncertainty, we perform a sensitivity analysis on the overall DAC cost, fixing the bounds for the adsorbent's cost coefficients to \$7−30 per kg for MIL-101(Cr)-PEI-800 and \$25−100 per kg for mmen-Mg_2(dobpdc). The lower bound corresponds to twice the adsorbent synthesis efficiency and the upper bound corresponds to 50% product yield for both the adsorbents. The lifetime of the adsorbent (N_{yr2}) is assumed to vary between 1 to 3 years for the sensitivity analysis. Figure 9 shows the variation of the adsorbent cost (C_5) with the cost coefficient (C_{ads}) and adsorbent lifetime (N_{yr1}) for the mmen-Mg_2(dobpdc) adsorbent.

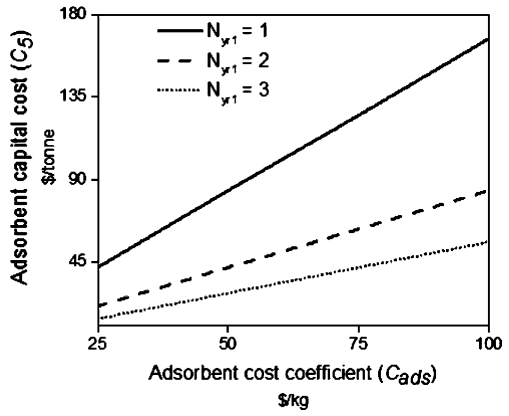

Figure 9. Variation of the adsorbent cost with the cost coefficient and adsorbent lifetime for the mmen-Mg_2(dobpdc) adsorbent.

Table 10 summarizes the contribution of each component that contributes to the total cost for the DAC process. The adsorbent capital cost, which includes the adsorbent's purchase cost and the lifetime of the adsorbent, is the parameter to which the total cost is most sensitive.

Table 10. Cost Components of the TVSA Model for DAC

cost components	value (\$/tonne) (MIL-101(Cr)-PEI-800)	value (\$/tonne) (mmen-Mg_2(dobpdc))
blowers (C_1)	24.0	20.0
steam (C_2)	15.0	5.0
vacuum pump opex (C_3)	2.0	1.0
monolith (C_4)	5.0	4.0
adsorbent (C_5)	5.0−70.0	10.0−140.0
blower (C_6)	15.0	10.0
vacuum pump capex (C_7)	9.0	10.0
total cost	75.0−140.0	60.0−190.0

6.5. Cyclic Step Times and Inlet Velocity Analysis. Increasing the monolithic wall thickness increases the energy penalty associated with heating up the wall during the desorption step. Figure 10a shows the permissible wall thickness (R_3-R_2) associated with monoliths of different cell density (cpsi). This unit represents the number of channels in the unit cross-sectional area of the monolith. It can be seen from the figure that the wall thickness decreases with an increase in cell density. Figure 10b shows the variation of the

DOI: 10.1021/acs.iecr.6b03887
Ind. Eng. Chem. Res. 2017, 56, 750−764

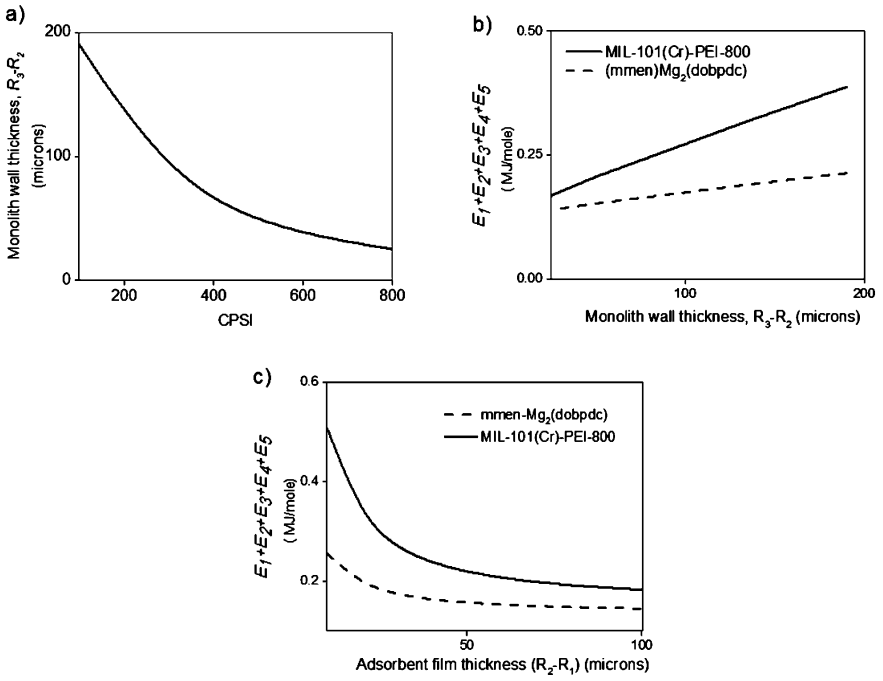

Figure 10. (a) Variation of monolith wall thickness with cpsi; (b) variation of minimum energy requirements with the wall thickness; and (c) variation of the minimum energy requirements with the adsorbent film thickness.

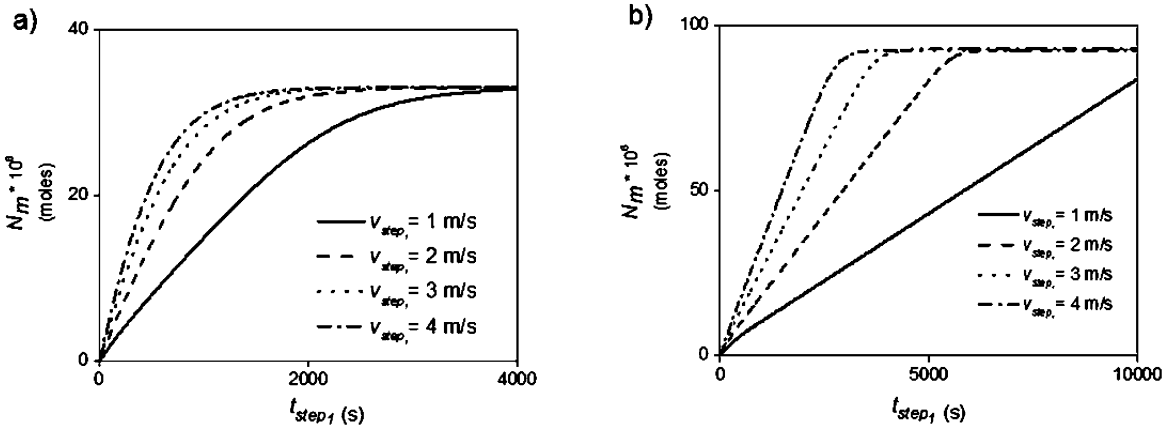

Figure 11. Total moles of CO_2 adsorbed during the adsorption step using (a) MIL-101(Cr)-PEI-800 and (b) mmen-Mg_2(dobpdc) adsorbents.

desorption step energy requirements with the wall thickness. As can be seen from the figure, the energy requirements during the desorption step decrease with a reduction in the wall thickness. This is due to the lower energy penalty required to heat the monolithic wall during the desorption step. Ideally, we would like as thin a monolithic wall as possible. However, decreasing the thickness of the wall reduces the structural stability of the monolith and reduces the manufacturing yields.

Increasing the thickness of the adsorbent film results in an increased amount of CO_2 being captured. This results in the reduction of the desorption step energy requirements (Joules per moles of CO_2 captured). Figure 10c shows the variation of the desorption step energy requirements with the adsorbent film thickness (R_2-R_1). As can be seen from the figure, the energy requirements during the desorption step decrease upon increasing the adsorbent film thickness.

To minimize the energy requirements, we would like to grow as thick a film as possible (refer Figure S6 in Supporting Information). However, increasing the adsorbent film thickness reduces its adherence stability to the wall. In the present analysis, we are assuming a 60-μm thick adsorbent film on a 400 cpsi monolithic substrate. The energy requirements can be further reduced if it is possible to grow an even thicker MOF film.

There are four additional parameters to which the overall cost of the process (operating and capital) appear to be most sensitive. These parameters are

1. air inlet velocity ($v_{\text{step }1}$) during the adsorption step
2. adsorption time ($t_{\text{step }1}$)
3. desorption time ($t_{\text{step }4}$)
4. steam inlet velocity ($v_{\text{step }4}$) during the desorption step

These parameters need to be chosen carefully to design a reasonable temperature vacuum swing process.

An efficient TVSA process needs to have the inlet air flow rate (v_{step}) during the adsorption step such that the cost and energy requirements are minimized. If the air flow rate is too small, the adsorption time increases since the entire adsorbent

DOI: 10.1021/acs.iecr.6b03887
Ind. Eng. Chem. Res. 2017, 56, 750−764

is not efficiently utilized, resulting in decreased productivity. On the other hand, if the air flow rate is too high, much of the CO_2 escapes the channel exit instead of being adsorbed. This results in an excessive power requirement to provide the high air flow rate.

The model is simulated for a single channel to study the effect of the air flow rate on the adsorption step. An analysis of the net CO_2 moles adsorbed per channel at different air flow rates is presented in Figure 11. Figure 11 analyzes the effect of the air velocity for the MIL-101(Cr)-PEI-800 and mmen-Mg_2(dobpdc) adsorbents. Both the figures show that on increasing the air velocity, the time taken for complete adsorption of CO_2 decreases. This happens because as the air flow rate increases the adsorbent productivity increases since the cycle time is reduced, thus allowing a larger amount of CO_2 to be fed per unit time. However, there is no significant change in the time for complete CO_2 adsorption when the air velocity is increased beyond 3 m/s. This is because at 3 m/s, the channel adsorbent surface is exposed to gaseous CO_2 molecules essentially for the entire adsorption step. Thus, an increase in air velocity beyond 3 m/s has negligible additional effect on the adsorption rate of CO_2.

To study the impact of the adsorption and desorption time and steam velocity on the cycle performance, eqs 12 and 13 defining the capture fractions during the adsorption step and desorption steps, α_1 and α_2, respectively, are used. The α_1 and α_2 are defined based on the first cycle and the adsorption and desorption time obtained is enforced on the remaining cycles to reach a cyclic steady state, as illustrated in Figure 12.

$$\alpha_1 = \frac{Q_1}{Q^{eq}_{CO_2|298\,K}} \tag{12}$$

$$\alpha_2 = \frac{Q_1 - Q_2}{Q^{eq}_{CO_2|298\,K}} \tag{13}$$

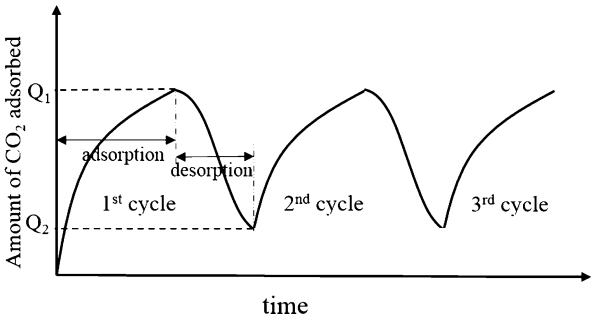

Figure 12. Illustration of the definitions of the parameters α_1 and α_2.

where α_1 is the adsorbed amount of CO_2 normalized by the equilibrium capacity and α_2 is the desorbed amount of CO_2 also normalized by the equilibrium capacity, $Q_1 = Q_{avg|t_{step\,1}}$ and $Q_2 = Q_{avg|(t_{step\,1} + t_{step\,2})}$.

Figure 13 shows the variation of the overall cost of the DAC process with the steam velocity ($v_{step\,4}$) for different combinations of α_1 and α_2 while keeping the air velocity at 3 m/s. It can be seen from the figure that a consistent minimum overall cost of DAC is obtained with a steam velocity at 0.04 m/s for the MIL-101(Cr)-PEI-800 adsorbents and ~0.1 m/s for the mmen-Mg_2(dobpdc) adsorbent.

The adsorption ($t_{step\,1}$) and desorption time ($t_{step\,4}$) should be determined so that these steps stop when the rate of adsorption (or desorption) per unit area (or flux, λ, as defined in eq 14) drops significantly (refer to section S7 in the Supporting Information).

$$\lambda = \rho_{ads}(1 - \varepsilon)\int_0^L \frac{dQ_{CO_2}}{dt}\,dz \tag{14}$$

To determine the adsorption ($t_{step\,1}$) and desorption times ($t_{step\,4}$), we performed an analysis on the variation of the overall DAC cost with α_1 for different α_2, keeping the air velocity at 3 m/s for both the adsorbents and the steam velocity at 0.04 m/s for MIL-101(Cr)-PEI-800, and 0.1 m/s for mmen-Mg_2(dobpdc). As can be seen from Figure 14, we get a consistent minimum cost when $\alpha_1 \sim 0.90$ and $\alpha_2 \sim 0.70$ for MIL-101(Cr)-PEI-800 and $\alpha_1 \sim 0.95$ and $\alpha_2 \sim 0.88$ for mmen-Mg_2(dobpdc). Further discussion on the economics of the TVSA model is presented in section 6.4.

All the results presented above are at the cyclic steady state. The final adsorption and desorption times selected for both the adsorbents are reported in Table 8.

The overall purities in the base cases for the MIL-101(Cr)-PEI-800 and mmen-Mg_2(dobpdc) adsorbents are 95%, defined on a steam free basis, and the recoveries of CO_2 are 50% and 60%, defined on air feed basis, respectively. The low recoveries are not of specific concern in DAC, because the feed is effectively free, while low purities may impact subsequent sequestration or utilization processes.

7. SUMMARY AND CONCLUSIONS

In this study, numerical modeling and simulation was used to analyze the performance of a TVSA process for DAC using a monolith structure coated with a MOF film. Isotherm parameter estimation for CO_2 adsorption was carried out for the MOFs MIL-101(Cr)-PEI-800 and mmen-Mg_2(dobpdc), which showed that the latter adsorbent had a significantly higher equilibrium capacity at the ambient CO_2 concentration (400 ppm). For the monolith structure, a wall thickness of 50 μm (corresponding to 400 cpsi) and a film thickness of 60 μm were chosen as design parameters. The TVSA process comprised five steps: adsorption, evacuation, pressurization, desorption, and cooling. System design parameters were determined by performing sensitivity analyses on the parameters of the key steps. The inlet air flow rate of 3 m/s was heuristically determined to be effective, and during desorption an inlet steam flow rate of 0.04 m/s for MIL-101(Cr)-PEI-800 and 0.1 m/s for mmen-Mg_2(dobpdc) was used. Adsorption and desorption times were determined for both the adsorbents, using an analysis of the amount of the equilibrium capacity used during adsorption, and the residual amount of CO_2 left after desorption, which together defined a swing capacity and where on the equilibrium curve this swing is located. These were 19 and 21 min for the adsorption and desorption for MIL-101(Cr)-PEI-800 and 1 h and 15 min for the mmen-Mg_2(dobpdc) adsorbent.

The energy requirements for the DAC process were determined. The minimum energy requirement for both the adsorbents, (0.145 MJ/mol for MIL-101(Cr)-PEI-800 and 0.113 MJ/mol for mmen-Mg_2(dobpdc)), is less than the energy associated with the heat of combustion that generated the CO_2 (0.45 MJ/mol). The energy requirements can be further reduced if we are able to experimentally grow thicker MOF

DOI: 10.1021/acs.iecr.6b03887
Ind. Eng. Chem. Res. 2017, 56, 750−764

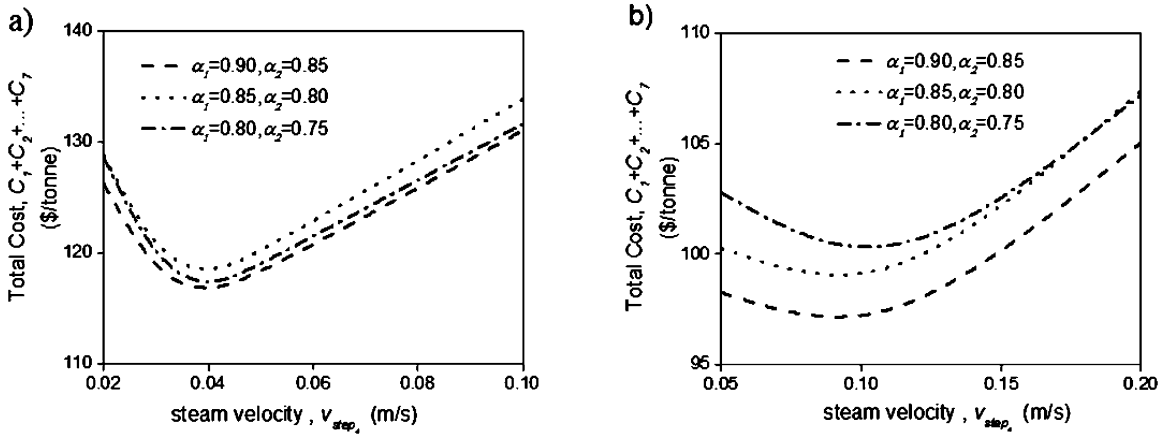

Figure 13. Variation of the overall cost of DAC with the steam velocity for (a) MIL-101(Cr)-PEI-800, (b) mmen-Mg_2(dobpdc) adsorbents.

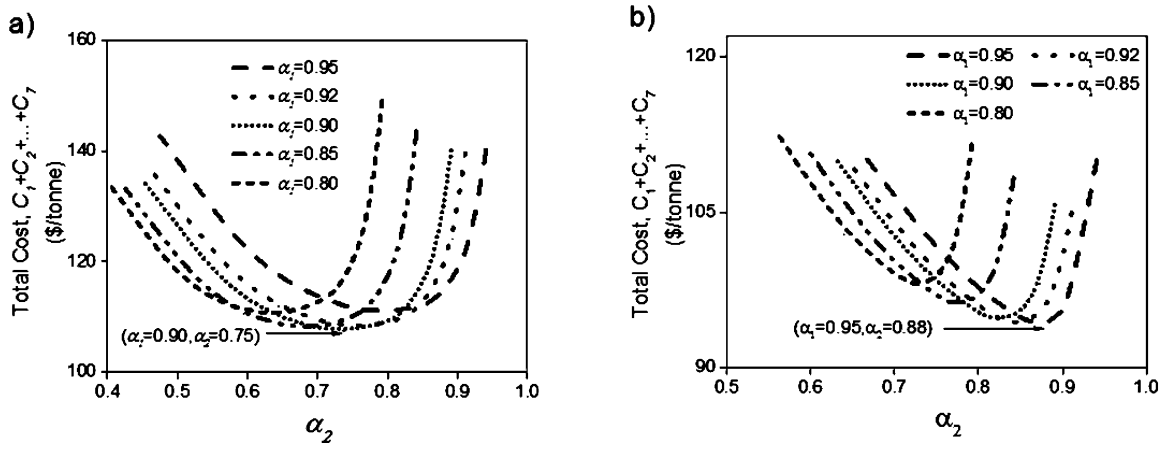

Figure 14. Variation of the overall cost of DAC with α_2 for different α_1 for (a) the MIL-101(Cr)-PEI-800 and (b) the mmen-Mg_2(dobpdc) adsorbents.

films and have thinner monolith walls structurally stable. We have also performed a detailed economic analysis for the Direct Air Capture. Various components for operating and capital costs were identified and the purchase cost of the adsorbent was identified as the key uncertain parameters in the TVSA model. It was found that the total cost for MIL-101(Cr)-PEI-800 is around \$75−140 per tonne of CO_2 captured if we consider the lifetime of adsorbent between 1 and 3 years. On the other hand, the net cost for mmen-Mg_2(dobpdc) is around \$60−190 per tonne of CO_2 captured for same range of adsorbent's lifetime.

Growing thicker adsorbent films and thinner monolithic walls can further reduce the net energy requirement (Figure 10b,c). Other ways to reduce these energy requirements is to look for better adsorbent candidates with higher equilibrium capacities at the ambient CO_2 concentration. Finally, in this analysis we assume that the steam was raised using traditional fuels; if the steam and electricity were provided via a solar thermal cycle (primary solar energy) the net sequestration potential of the process, the difference between the CO_2 captured versus the CO_2 spent in capturing it, could be further improved. Further optimization study with additional parameters such as channel length, film, and wall thickness needs to be performed on the proposed model, and recovery of heat from the steam through heat integration will further improve the energy and cost estimates for the process. Diffusivity of CO_2 inside the adsorbent also needs to be determined experimentally for more accurate analysis. Checking thermal stability of the MOFs in the long term cycle test (for determining lifetime of the adsorbent) is also a key issue which needs to be addressed in future studies.

In conclusion, the analysis presented in this paper provides a promising step toward the scientific efforts in the field of DAC.[4−7] Our work is the first attempt to address detailed energy and cost estimates of DAC through the comprehensive modeling study of a TVSA process using MOF adsorbent films on a monolithic substrate.

■ ASSOCIATED CONTENT

Supporting Information

The Supporting Information is available free of charge on the ACS Publications website at DOI: 10.1021/acs.iecr.6b03887.

Model equations, energy requirement derivations, cost requirements derivations, isotherm parameter estimation (Figure S1), heat transfer coefficient calculation, evacuation and pressurization steps (Figures S2 and S3), model cyclic simulation analysis (Figure S4), flux analysis during adsorption and desorption step (Figure S5), film growth on monolithic substrate (Figure S6) (PDF)

DOI: 10.1021/acs.iecr.6b03887
Ind. Eng. Chem. Res. 2017, 56, 750−764

AUTHOR INFORMATION

Corresponding Author

* E-mail: ykawajiri@chbe.gatech.edu. Tel.: +1 (404) 894-2856. Fax: (404) 894-2866.

ORCID

Anshuman Sinha: 0000-0001-6661-1013
Lalit A. Darunte: 0000-0001-6086-8520
Christopher W. Jones: 0000-0003-3255-5791
Yoshiaki Kawajiri: 0000-0002-7124-1704

Notes

The authors declare no competing financial interest.

ACKNOWLEDGMENTS

This material is based upon work supported by the National Science Foundation (CBET-1336386). The authors would like to thank Jeffrey R. Long and Thomas McDonald of UC Berkeley for kindly providing the raw data of the measured CO_2 adsorption isotherms.[45]

NOMENCLATURE

C_j = concentration of the component j in the gas phase in the channel
$C^i_{H_2O}$ = concentration of condensed water at the interface
v = velocity of the gas in the channel
L = length of the channel (0.3 m)
R_1 = inner radius of the adsorbent film (0.000525 m)
R_2 = outer radius of the adsorbent film (0.000585 m)
R_3 = outer radius of the monolith wall (0.000635 m)
D_j = diffusivity of the component j in the channel
ρ_w = density of the component w
k_w = thermal conductivity of component w
$Q^{eq}_{CO_2}$ = equilibrium concentration of CO_2 at the adsorbent surface
Q_{CO_2} = bulk concentration of adsorbed CO_2
T_w = temperature of the component w
As_1 = specific surface area of the adsorbent
As_2 = specific surface area of the monolith wall
$C_{p,w}$ = specific heat of the component w
h = heat transfer coefficient
$L^{vap}_{H_2O}$ = latent heat of vaporization of water
H_{vap} = heat transferred during evaporation/condensation of water vapor
Q_{gen} = heat transferred during adsorption/desorption of CO_2
Q_{avg} = average amount of CO_2 adsorbed in the adsorbent
P = total pressure inside the channel
N_m or N_t = amount of CO_2 in moles (m) or tonnes (t)
R = gas constant
k = overall mass transfer coefficient
k_i/k_e = internal/external mass transfer coefficient
λ = flux of CO_2 during adsorption and desorption step

Subscript

CO_2 = carbon dioxide
inert = inert gases (N_2 and O_2)
H_2O = water vapor
gas = gas present in the channel
ads = adsorbent
wall = monolithic wall

REFERENCES

(1) Canadell, J. G.; L, Q. C.; Raupach, M. R.; Field, C. B.; Buitenhuis, E. T.; Ciais, P.; Conway, T. J.; Gillett, N. P.; Houghton, R. A.; Marland, G. Contributions to accelerating atmospheric CO2 growth from economic activity, carbon intensity, and efficiency of natural sinks. *Proc. Natl. Acad. Sci. U. S. A.* **2007**, *104* (47), 18866−70.
(2) Intergovernmental Panel on Climate Change. *Climate Change 2014: Mitigation of Climate Change*; Cambridge University Press, 2015; Vol. 3.
(3) Jones, C. W. CO2 capture from dilute gases as a component of modern global carbon management. *Annu. Rev. Chem. Biomol. Eng.* **2011**, *2*, 31−52.
(4) Greenwood, K.; Pearce, M. The removal of carbon dioxide from atmospheric air by scrubbing with caustic soda in packed towers. *Chem. Eng. News* **1953**, *31*, 201−207.
(5) Spector, N. A.; Dodge, B. F. Removal of carbon dioxide from atmospheric air. *Trans. Am. Inst. Chem. Eng.* **1946**, *42* (5−6), 827−848.
(6) Tepe, J. B.; Dodge, B. F. Absorption of carbon dioxide by sodium hydroxide solutions in a packed column. *Trans. Am. Inst. Chem. Eng.* **1943**, *39*, 255−276.
(7) Lackner, K. S.; Grimes, P.; Ziock, H.-J. Carbon dioxide extraction from air: is it an option? *24th Ann. Tech. Conf. Coal Utilization* **1999**, 885−896.
(8) Lackner, K. S.; Brennan, S.; Matter, J. M.; Park, A. H. A.; Wright, A.; Van Der Zwaan, B. The urgency of the development of CO2 capture from ambient air. *Proc. Natl. Acad. Sci. U. S. A.* **2012**, *109* (33), 13156−13162.
(9) Zeman, F. Energy and Material Balance of CO2 Capture from Ambient Air. *Environ. Sci. Technol.* **2007**, *41*, 7558−7563.
(10) Zeman, F. S.; Lackner, K. S. Capturing carbon dioxide directly from the atmosphere. *World Resour. Rev.* **2004**, *16*, 157−172.
(11) Baciocchi, R.; Storti, G.; Mazzotti, M. Process design and energy requirements for the capture of carbon dioxide from air. *Chem. Eng. Process.* **2006**, *45* (12), 1047−1058.
(12) Mahmoudkhani, M.; Keith, D. W. Low-energy sodium hydroxide recovery for CO2 capture from atmospheric air—Thermodynamic analysis. *Int. J. Greenhouse Gas Control* **2009**, *3* (4), 376−384.
(13) Stolaroff, J. K.; Keith, D. W.; Lowry, G. V. Carbon Dioxide Capture from Atmospheric Air Using Sodium Hydroxide Spray. *Environ. Sci. Technol.* **2008**, *42*, 2728−2735.
(14) Yuan, Z.; Eden, M. R.; Gani, R. Toward the Development and Deployment of Large-Scale Carbon Dioxide Capture and Conversion Processes. *Ind. Eng. Chem. Res.* **2015**, *55* (12), 3383−3419.
(15) Didas, S. A.; Choi, S.; Chaikittisilp, W.; Jones, C. W. Amine−Oxide Hybrid Materials for CO2 Capture from Ambient Air. *Acc. Chem. Res.* **2015**, *48* (10), 2680−2687.
(16) Darunte, L. A.; Walton, K. S.; Sholl, D. S.; Jones, C. W. CO2 capture via adsorption in amine-functionalized sorbents. *Curr. Opin. Chem. Eng.* **2016**, *12*, 82−90.
(17) Sanz-Pérez, E. S.; Murdock, C. R.; Didas, S. A.; Jones, C. W. Direct Capture of CO2 from Ambient Air. *Chem. Rev.* **2016**, *116*, 11840.
(18) Simon, A. J.; Kaahaaina, N. B.; Friedmann, S. J.; Aines, R. D. Systems analysis and cost estimates for large scale capture of carbon dioxide from air. *Energy Procedia* **2011**, *4*, 2893−2900.
(19) Smith, P.; Davis, S. J.; Creutzig, F.; Fuss, S.; Minx, J.; Gabrielle, B.; Kato, E.; Jackson, R. B.; Cowie, A.; Kriegler, E.; Van Vuuren, D. P. Biophysical and economic limits to negative CO2 emissions. *Nature Climate Change* **2016**, *6* (1), 42−50.
(20) House, K. Z.; Baclig, A. C.; Ranjan, M.; van Nierop, E. A.; Wilcox, J.; Herzog, H. J. Economic and energetic analysis of capturing CO2 from ambient air. *Proc. Natl. Acad. Sci. U. S. A.* **2011**, *108* (51), 20428−20433.
(21) Realff, M. J.; Eisenberger, P. Flawed analysis of the possibility of air capture. *Proc. Natl. Acad. Sci. U. S. A.* **2012**, *109* (25), E1589.
(22) Socolow, R. A Technology Assessment for the APS Panel on Public Affairs, American Physical Society. *Phys. Today* **2011**, *39*, 60.
(23) Zeman, F. Reducing the cost of Ca-based direct air capture of CO2. *Environ. Sci. Technol.* **2014**, *48* (19), 11730−11735.

DOI: 10.1021/acs.iecr.6b03887
Ind. Eng. Chem. Res. 2017, 56, 750−764

(24) Kulkarni, A. R.; Sholl, D. S. Analysis of Equilibrium-Based TSA Processes for Direct Capture of CO2from Air. *Ind. Eng. Chem. Res.* **2012**, *51* (25), 8631−8645.
(25) Darunte, L. A.; Oetomo, A. D.; Walton, K. S.; Sholl, D. S.; Jones, C. W. Direct Air Capture of CO2 using Amine Functionalized MIL-101 (Cr). *ACS Sustainable Chem. Eng.* **2016**, *4*, 5761−5768.
(26) Buzanowski, M. A.; Rege, S. U.; Yang, R. Y. Sorbents for air prepurification in air separation. *Chem. Eng. Sci.* **2000**, *55*, 4827−4838.
(27) Buzanowski; Rege, S. U.; Yang, R. T.; Qian, K. Air-prepurification by pressure swing adsorption using single/layered beds. *Chem. Eng. Sci.* **2001**, *56*, 2745−2759.
(28) Wang, Q.; Luo, J.; Zhong, Z.; Borgna, A. CO2 capture by solid adsorbents and their applications: current status and new trends. *Energy Environ. Sci.* **2011**, *4* (1), 42−55.
(29) Lively, R. P.; Realff, M. J. On thermodynamic separation efficiency: Adsorption processes. *AIChE J.* **2016**, *62*, 3699.
(30) Yu, C.-H.; Huang, C.-H.; Tan, C.-S. A Review of CO2 Capture by Absorption and Adsorption. *Aerosol Air Qual. Res.* **2012**, DOI: 10.4209/aaqr.2012.05.0132.
(31) Liu, J.; Tian, J.; Thallapally, P. K.; McGrail, B. P. Selective CO2Capture from Flue Gas Using Metal−Organic Frameworks——A Fixed Bed Study. *J. Phys. Chem. C* **2012**, *116* (17), 9575−9581.
(32) Sumida, K.; Rogow, D. L.; Mason, J. A.; McDonald, T. M.; Bloch, E. D.; Herm, Z. R.; Bae, T. H.; Long, J. R. Carbon dioxide capture in metal-organic frameworks. *Chem. Rev.* **2012**, *112* (2), 724−81.
(33) Saha, D.; Bao, Z.; Jia, F.; Deng, S. Adsorption of CO2, CH4, N2O, and N2 on MOF-5, MOF-177, and Zeolite 5A. *Environ. Sci. Technol.* **2010**, *44*, 1820−1826.
(34) Yazaydın, A. O.; Snurr, R. Q.; Park, T. H.; Koh, K.; Liu, J.; LeVan, M. D.; Benin, A. I.; Jakubczak, P.; Lanuza, M.; Galloway, D. B.; Low, J. J.; Willis, R. R. Screening of Metal-Organic Frameworks for Carbon Dioxide Capture from Flue Gas Using a Combined Experimental and Modeling Approach. *J. Am. Chem. Soc.* **2009**, *131*, 18198−18199.
(35) Yaghi, O. M.; Millward, A. R. Metal-Organic Frameworks with Exceptionally High Capacity for Storage of Carbon Dioxide at Room Temperature. *J. Am. Chem. Soc.* **2005**, *127*, 17998−17999.
(36) Li, J. R.; Kuppler, R. J.; Zhou, H. C. Selective gas adsorption and separation in metal-organic frameworks. *Chem. Soc. Rev.* **2009**, *38* (5), 1477−504.
(37) Kuppler, R. J.; Timmons, D. J.; Fang, Q.-R.; Li, J.-R.; Makal, T. A.; Young, M. D.; Yuan, D.; Zhao, D.; Zhuang, W.; Zhou, H.-C. Potential applications of metal-organic frameworks. *Coord. Chem. Rev.* **2009**, *253* (23−24), 3042−3066.
(38) Belmabkhout, Y.; Serna-Guerrero, R.; Sayari, A. Amine-bearing mesoporous silica for CO2 removal from dry and humid air. *Chem. Eng. Sci.* **2010**, *65* (11), 3695−3698.
(39) Bao, Z.; Yu, L.; Ren, Q.; Lu, X.; Deng, S. Adsorption of CO2 and CH4 on a magnesium-based metal organic framework. *J. Colloid Interface Sci.* **2011**, *353* (2), 549−56.
(40) Hong, D. Y.; Hwang, Y. K.; Serre, C.; Ferey, G.; Chang, J. S. Porous Chromium Terephthalate MIL-101 with Coordinatively Unsaturated Sites: Surface Functionalization, Encapsulation, Sorption and Catalysis. *Adv. Funct. Mater.* **2009**, *19* (10), 1537−1552.
(41) Lin, Y.; Yan, Q.; Kong, C.; Chen, L. Polyethyleneimine incorporated metal-organic frameworks adsorbent for highly selective CO2 capture. *Sci. Rep.* **2013**, *3*, 1859.
(42) Lin, Y.; Lin, H.; Wang, H.; Suo, Y.; Li, B.; Kong, C.; Chen, L. Enhanced selective CO 2 adsorption on polyamine/MIL-101 (Cr) composites. *J. Mater. Chem. A* **2014**, *2* (35), 14658−14665.
(43) McDonald, T. M.; Lee, W. R.; Mason, J. A.; Wiers, B. M.; Hong, C. S.; Long, J. R. Capture of carbon dioxide from air and flue gas in the alkylamine-appended metal-organic framework mmen-Mg2(dobpdc). *J. Am. Chem. Soc.* **2012**, *134* (16), 7056−65.
(44) Mason, J. A.; Sumida, K.; Herm, Z. R.; Krishna, R.; Long, J. R. Evaluating metal−organic frameworks for post-combustion carbon dioxide capture via temperature swing adsorption. *Energy Environ. Sci.* **2011**, *4* (8), 3030.
(45) McDonald, T. M.; Mason, J. A.; Kong, X.; Bloch, E. D.; Gygi, D.; Dani, A.; Crocellà, V.; Giordanino, F.; Odoh, S. O.; Drisdell, W. S.; Vlaisavljevich, B. Cooperative insertion of CO2 in diamine-appended metal-organic frameworks. *Nature* **2015**, *519* (7543), 303−308.
(46) Rezaei, F.; Subramanian, S.; Kalyanaraman, J.; Lively, R. P.; Kawajiri, Y.; Realff, M. J. Modeling of rapid temperature swing adsorption using hollow fiber sorbents. *Chem. Eng. Sci.* **2014**, *113*, 62−76.
(47) Lively, R. P.; Chance, R. R.; Kelley, B. T.; Deckman, H. W.; Drese, J. H.; Jones, C. W.; Koros, W. J. Hollow fiber adsorbents for CO2 removal from flue gas. *Ind. Eng. Chem. Res.* **2009**, *48* (15), 7314−7324.
(48) Casas, N.; Schell, J.; Joss, L.; Mazzotti, M. A parametric study of a PSA process for pre-combustion CO2 capture. *Sep. Purif. Technol.* **2013**, *104*, 183−192.
(49) Wurzbacher, J. A.; Gebald, C.; Piatkowski, N.; Steinfeld, A. Concurrent separation of CO2 and H2O from air by a temperature-vacuum swing adsorption/desorption cycle. *Environ. Sci. Technol.* **2012**, *46* (16), 9191−8.
(50) Hefti, M.; Joss, L.; Bjelobrk, Z.; Mazzotti, M. On the potential of phase-change adsorbents for CO2 capture by temperature swing adsorption. *Faraday Discuss.* **2016**, *192*, 153.
(51) Yates, M.; Blanco, J.; Martin-Luengo, M. A.; Martin, M. P. Vapour adsorption capacity of controlled porosity honeycomb monoliths. *Microporous Mesoporous Mater.* **2003**, *65* (2−3), 219−231.
(52) Yu, F. D.; Luo, L. A.; Grevillot, G. Adsorption Isotherms of VOCs onto an Activated Carbon Monolith: Experimental Measurement and Correlation with Different Models. *J. Chem. Eng. Data* **2002**, *47*, 467−473.
(53) Li, Y. Y.; Perera, S. P.; Crittenden, B. D. Zeolite monoliths for air separation Part 2: Oxygen Enrichment, Pressure Drop and Pressurization. *Trans IChemE* **1998**, *76* (8), 931−941.
(54) Rezaei, F.; Webley, P. Optimum structured adsorbents for gas separation processes. *Chem. Eng. Sci.* **2009**, *64* (24), 5182−5191.
(55) Rezaei, F.; Webley, P. Structured adsorbents in gas separation processes. *Sep. Purif. Technol.* **2010**, *70* (3), 243−256.
(56) Rezaei, F.; Mosca, A.; Hedlund, J.; Webley, P. A.; Grahn, M.; Mouzon, J. The effect of wall porosity and zeolite film thickness on the dynamic behavior of adsorbents in the form of coated monoliths. *Sep. Purif. Technol.* **2011**, *81* (2), 191−199.
(57) Sakwa-Novak, M. A.; Jones, C. W. Steam induced structural changes of a poly(ethylenimine) impregnated gamma-alumina sorbent for CO2 extraction from ambient air. *ACS Appl. Mater. Interfaces* **2014**, *6* (12), 9245−55.
(58) Hammache, S.; Hoffman, J. S.; Gray, M. L.; Fauth, D. J.; Howard, B. H.; Pennline, H. W. Comprehensive Study of the Impact of Steam on Polyethyleneimine on Silica for CO2Capture. *Energy Fuels* **2013**, *27* (11), 6899−6905.
(59) Li, W.; Bollini, P.; Didas, S. A.; Choi, S.; Drese, J. H.; Jones, C. W. Structural changes of silica mesocellular foam supported amine-functionalized CO2 adsorbents upon exposure to steam. *ACS Appl. Mater. Interfaces* **2010**, *2* (11), 3363−72.
(60) Chaikittisilp, W.; Kim, H.-J.; Jones, C. W. Mesoporous Alumina-Supported Amines as Potential Steam-Stable Adsorbents for Capturing CO2from Simulated Flue Gas and Ambient Air. *Energy Fuels* **2011**, *25* (11), 5528−5537.
(61) Li, W.; Choi, S.; Drese, J. H.; Hornbostel, M.; Krishnan, G.; Eisenberger, P. M.; Jones, C. W. Steam-stripping for regeneration of supported amine-based CO(2) adsorbents. *ChemSusChem* **2010**, *3* (8), 899−903.
(62) Bollini, P.; Choi, S.; Drese, J. H.; Jones, C. W. Oxidative degradation of aminosilica adsorbents relevant to postcombustion CO2 capture. *Energy Fuels* **2011**, *25* (5), 2416−2425.
(63) Heydari-Gorji, A.; Sayari, A. Thermal, Oxidative, and CO2-Induced Degradation of Supported Polyethylenimine Adsorbents. *Ind. Eng. Chem. Res.* **2012**, *51* (19), 6887−6894.
(64) Bird, R. B.; Stewart, W. E.; Lightfoot, E. N. *Transport Phenomena*; Wiley: New York, 1960.

DOI: 10.1021/acs.iecr.6b03887
Ind. Eng. Chem. Res. 2017, 56, 750−764

(65) Patton, A.; Crittenden, B. D.; Perera, S. P. Use of the linear driving force approximation to guide the design of monolithic adsorbents. *Chem. Eng. Res. Des.* **2004**, *82* (8), 999−1009.
(66) Jeong, K.; Kessen, M. J.; Bilirgen, H.; Levy, E. K. Analytical modeling of water condensation in condensing heat exchanger. *Int. J. Heat Mass Transfer* **2010**, *53* (11), 2361−2368.
(67) Liu, D.; Purewal, J. J.; Yang, J.; Sudik, A.; Maurer, S.; Mueller, U.; Ni, J.; Siegel, D. J. MOF-5 composites exhibiting improved thermal conductivity. *Int. J. Hydrogen Energy* **2012**, *37* (7), 6109−6117.
(68) Huang, B. L.; Ni, Z.; Millward, A.; McGaughey, A. J. H.; Uher, C.; Kaviany, M.; Yaghi, O. Thermal conductivity of a metal-organic framework (MOF-5): Part II. Measurement. *Int. J. Heat Mass Transfer* **2007**, *50* (3), 405−411.
(69) Osborne, D. W.; Schreiner, F.; Malm, J. G.; Selig, H.; Rochester, L. Heat Capacity and Other Thermodynamic Properties of MoF6 between 4° and 350° K. *J. Chem. Phys.* **1966**, *44* (7), 2802−2809.
(70) *Cordierite Ceramic Material: CoorsTek Technical Ceramics*; CoorsTek, 2016
(71) Carey, J. W. The heat capacity of hydrous cordierite above 295 K. *Phys. Chem. Miner.* **1993**, *19* (8), 578−583.
(72) Bridgeman, O. C.; Aldrich, E. W. Vapor pressure tables for water. *J. Heat Transfer* **1964**, *86* (2), 279−286.
(73) Saha, D.; Bao, Z.; Jia, F.; Deng, S. Adsorption of CO2, CH4, N2O, and N2 on MOF-5, MOF-177, and zeolite 5A. *Environ. Sci. Technol.* **2010**, *44* (5), 1820−1826.
(74) Li, J. R.; Ma, Y.; McCarthy, M. C.; Sculley, J.; Yu, J.; Jeong, H. K.; Balbuena, P. B.; Zhou, H. C. Vancouver, Carbon dioxide capture-related gas adsorption and separation in metal-organic frameworks. *Coord. Chem. Rev.* **2011**, *255* (15), 1791−1823.
(75) Zhao, Z.; Li, Z.; Lin, Y. S. Adsorption and diffusion of carbon dioxide on metal− organic framework (MOF-5). *Ind. Eng. Chem. Res.* **2009**, *48* (22), 10015−10020.
(76) Yang, R. T. *Gas Separation by Adsorption Processes*; Butterworth-Heinemann, 2013
(77) Independent Statistics and Analysis*Ann. Energy Rev.*; U.S. Energy Information Administration, EIA, 2016.
(78) DeSantis, D.; James, B. D.; Houchins, C.; Mason, J. A.; Veenstra, M.; Long, J. R. Techno-economic analysis of metal-organic frameworks for hydrogen and natural gas storage. *Environ. Sci. Technol.* **2016**, Accepted.

DOI: 10.1021/acs.iecr.6b03887
Ind. Eng. Chem. Res. 2017, 56, 750−764